Surface & Coatings Technology 447 (2022) 128826

Contents lists available at ScienceDirect

Surface & Coatings Technology

journal homepage: www.elsevier.com/locate/surfcoat

Roll-to-roll manufacture of flexible thin-film thermoelectric generators using flexography with vacuum vapour deposition

Xudong Tao, Bryan W. Stuart, Hazel E. Assender *

Department of Materials, University of Oxford, Parks Road, OX1 3PH, United Kingdom

ARTICLE INFO

Keywords:
Roll-to-roll
Flexible thermoelectric generator
Thin film
In-line patterning
Flexography technique
Physical vapour deposition

ABSTRACT

Exploring processes for industrial large-scale manufacture of low-cost electronic devices is timely for the upcoming era of the Internet of Things. In this study, a roll-to-roll process using selective metallisation (a combination of flexographic printing of an oil liquid-mask and physical vapour deposition: sputtering and evaporation) is explored for the large-scale manufacture of flexible electronics, with a wearable thermoelectric generator as an exemplar device. Two post-treatments (electron beam and infrared) are trialled to remove the residual oil after selective metallisation. Both are effective for the removal of oil, however, the oil used in selective metallisation degrades the functional thermoelectric material severely, causing a dramatic increase in the internal resistance of the device. This is attributable to (1) the doping and oxidation issues in the semiconductor film; (2) the existence of oil at the interface between the two coatings. The fabricated thermoelectric generator with post-treatments shows a good voltage output comparable to a standard device fabricated using shadow mask, providing an option for portable devices requiring a voltage source. This study reports an industrially compatible roll-to-roll manufacturing process for large-scale manufacture of flexible electronics. Further studies are under way to optimise the device performance.

1. Introduction

Flexible electronics technology has attracted great attention in the era of the Internet of Things [1]. Flexible electronics is a collective term for all kinds of electronic systems that are bendable and foldable [2]. Flexible technology has a wearable application that enables sensors/electronics to be implanted into the human body (e.g. a brain chip, *Neuralink*) or attached to human skin (e.g. a fitness tracker, *Fitbit® Flex™*). Flexible/wearable thermoelectric generators (TEGs) can be a local power source to minimise charging and energy storage requirements for wearable electronics [3]. TEGs exploit the Seebeck effect to generate power using a temperature difference (ΔT) between the human body temperature and the environment across thermoelectric (TE) semiconductors (e.g. bismuth telluride, Bi—Te, a typical kind of TE material that works in the human body-temperature range). Flexible thin-film TEGs made up of inorganic materials deposited onto a polymer substrate, are particularly attractive since nanostructured materials using boundary or defect engineering could significantly improve the performance of TE materials [4–7]. A wide variety of studies have been carried out around flexible thin-film TEGs since the first report in 2001 [8]. Physical vapour deposition techniques such as sputtering or evaporation are atomistic techniques [9] and have been widely used in the fabrication of inorganic flexible thermoelectric thin-film materials [9–11]. Physical vapour deposition techniques are roll-to-roll (R2R) compatible and have been applied in industry e.g. for flexible packaging [12]. Herein, this study focuses on an engineering challenge for large-scale manufacture in commercialisation: how to make in-line-deposited patterns for a flexible TEG using an industrially compatible process – physical vapour deposition in R2R.

R2R manufacture of flexible electronics is a developing field as a low-cost and high throughput means for technology transfer from laboratory to industry. Flexible TEGs can be printed onto flexible substrates on rollers in a fast R2R process using e.g. screen-printing [13,14], inkjet printing [15], or dispenser printing [16]. However, these solution-based printing techniques have an inherent drawback for fabricating thin-film TEGs: the film thickness cannot reach the nano-size range. However, nanostructured TEGs give the prospect of significantly improved device performance. Recent advances in a combination of flexography oil masking technique and thermal evaporation (the so-called selective metallisation technique, SMT [17]) raise the prospect of means to

* Corresponding author.
E-mail address: hazel.assender@materials.ox.ac.uk (H.E. Assender).

https://doi.org/10.1016/j.surfcoat.2022.128826
Received 28 July 2022; Received in revised form 23 August 2022; Accepted 23 August 2022
Available online 29 August 2022

fabricate in-line patterns of nano-thick metals in a fast (e.g. ~25 m min^{-1} in-line speed) R2R process for flexible electronics. In SMT, an oil mask is printed onto a polymer web, then the metal vapour is deposited by evaporation during which the oil is simultaneously evaporated by source radiative heating and metal condensation [17].

In addition to evaporation, sputtering is another promising technique for large-scale manufacturing because of its easy incorporation in R2R [18] and compatibility with in-line fabrication [19,20]. Typically, evaporation of functional materials (e.g. Bi—Te) requires multiple co-evaporation boats and power systems for each element, while sputtering is much easier for accurate process control of the deposition of functional thin films. Often superior functional properties can be achieved with sputtered layers and hence sputtering is widely industrially applied despite typically being orders of magnitude slower than can be achieved with evaporation. Further study using SMT by sputtering [21] demonstrated a successful in-line pattern of flexible electrodes for TEGs, however, the heating of oil on the substrate was insufficient during the sputter deposition to form a vapour cloud, and/or the vastly greater kinetic energy of the incoming particles via sputtering (several hundred eV compared to <1 eV for evaporation) prevented the oil vapour cloud from repelling depositing atoms/molecules such that the sputtered metal (in that case) deposited onto or into the oil. The residual oil remained, and thus a post-cleaning process (isopropanol washing) was required. Chemical solution washing is not a desired method in thin-film manufacturing because of the likely damage to nanostructures and the economics of the process. Hence, this study carries out a further study of the combination of SMT with sputtering. The previous work employed this technique to fabricate metal patterns while this study is the first trial

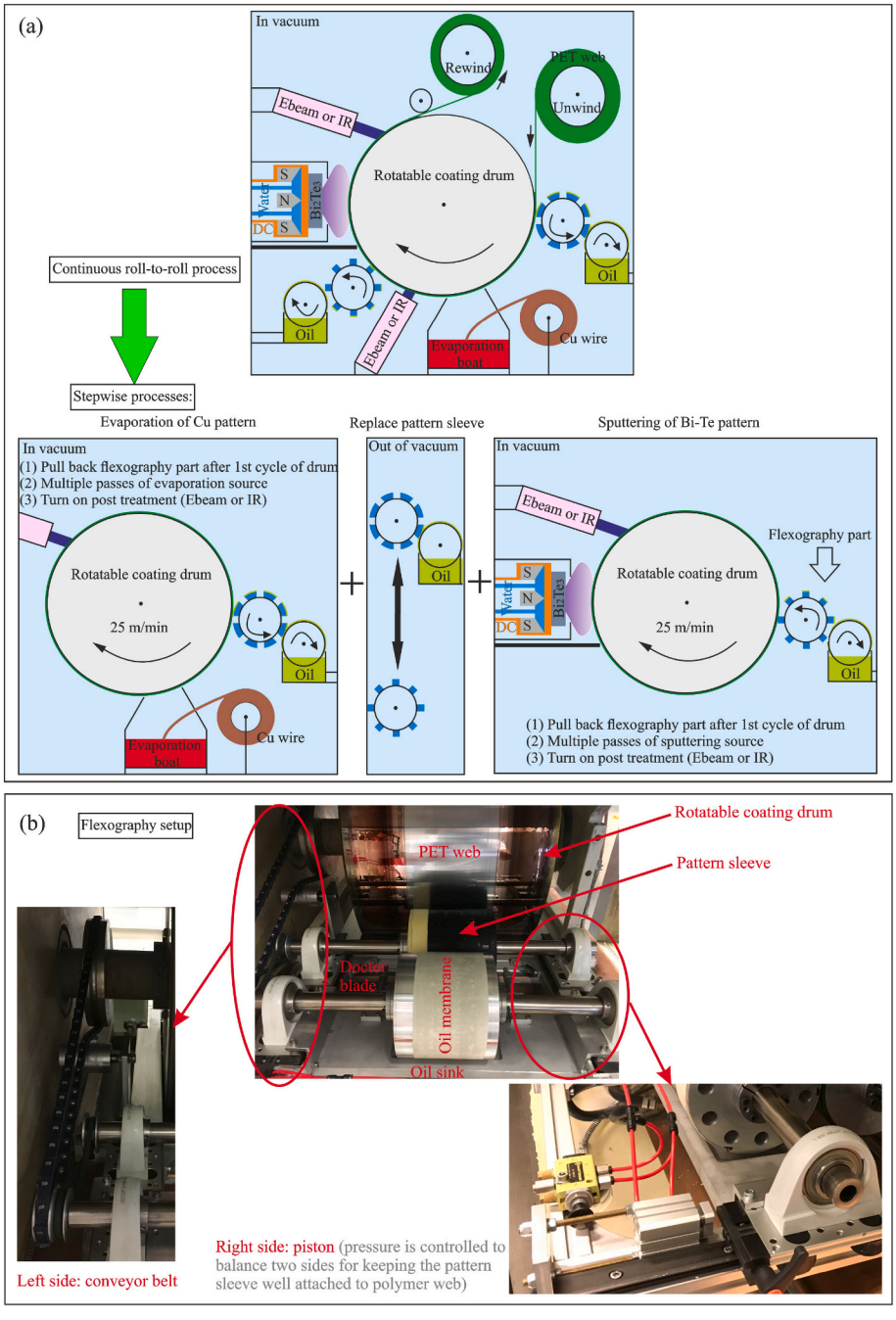

Fig. 1. (a) Schematics of continuous R2R setups and stepwise processes used in this work where SMT with evaporation of Cu was made in three individual processes: flexography + evaporation (2 cycles) + post-deposition treatment; the oil pattern plate of Cu was replaced with one for the Bi—Te pattern; SMT with sputtering (20 cycles) of Bi—Te was also made followed by post-deposition treatment to remove oil. (b) An image of flexography setup (with conveyor belt at left side and piston at right side to balance the pattern plate).

of this technique to fabricate patterned semiconductor materials.

In this study, SMT employs *Krytox*® vacuum oil as the liquid mask. The oil has a vapour temperature in a vacuum as shown in Appendix Fig. A. Hence, post-deposition heat treatment can be considered to remove residual oil. A vacuum oven [22–26] is the most simple and common method but it is not compatible with flexible polymer substrates in R2R, considering the blocking/melting risk of polymer roll. Two feasible post-annealing strategies, electron beam (Ebeam) and infrared (IR) irradiations, are proposed in this study to remove the residual oil without damage to the functional coating and polymer substrate. This would be a step closer to R2R high-throughput manufacture of flexible electronics for commercialisation.

2. Experimental details

2.1. Sample fabrication

To make the fabrication process easy, a single n-type TEG [27], rather than n- & p-type TEG [28], was employed in this study. Cu electrodes have been found favourable for electrically connecting the TE (Bi—Te) strips [29]. These semiconductor strips were electrically connected in series and a ΔT was applied in parallel to diffuse carriers from the hot side to the cold side [30].

A continuous R2R process was broken into stepwise processes as shown in Fig. 1 a. SMT with evaporation was used to make in-line patterns of Cu electrodes, followed by IR or Ebeam irradiation to remove the residual oil. Then, the oil printing pattern plate was replaced by one suitable for the pattern of the TE material layer. SMT with sputtering was then used to make patterns of Bi—Te films aligned to the previously deposited Cu patterns, followed by post-deposition treatments (Ebeam or IR) for removal of the residual oil. The flexography head was pulled back after the first rotation of the drum so it had deposited the oil pattern on the flexible sheet, then multiple passes of the oiled substrate were conducted over the deposition source for the film deposition and simultaneous removal of oil, followed by an IR or Ebeam treatment for completion of oil removal.

All films were fabricated onto a 125 μm-thick polyethylene terephthalate (PET) substrate in an *Aerre Machines* vacuum R2R webcoater under a base pressure of 1.3×10^{-4} mbar. Polymer web was attached to a coating drum (circumference 1.8 m) rotating at a speed of 25 m min^{-1} at the drum surface. In addition, silicon wafers were taped alongside the PET substrate to simultaneously make samples on which to measure the film thickness and for x-ray diffraction (XRD) characterisation.

The coating thickness was built up by multiple passes of the sputtering (20 passes) or evaporation (2 passes) source. The sputtering condition has been optimised from the previous study [31] (Ar flow rate: 250 sccm, DC power: 0.25 kW), using a three-inch planar Bi_2Te_3 target (99.999 % purity, *Mi-Net Technology Ltd.*). In terms of the evaporation, Cu wire (1.2 mm diameter, *Speedmet 98 Welding Alloys*) was fed into two resistively heated ceramic boats (*Sintec Ceramics*) for thermal evaporation under a power of ~500 A and a source-to-substrate of ~180 mm.

Both Ebeam (100 mA, 4 V) and IR (250 W) sources inside *Aerre Machine* vacuum R2R webcoater were trialled to remove residual oil from the patterning process with the sample attached to a rotating drum (25 m min^{-1}) under a vacuum of 1.3×10^{-4} mbar. ~12 min were required to reach the set condition for both Ebeam and IR, and ~5 min to cool down the sample before it was removed. The treatment time was varied: 1, 10, 25, and 50 min (a shorter time is desirable for a fast R2R process). The IR source was measured to heat a thermocouple at the coating drum to ~70 °C, close to the vaporisation temperature of *Krytox*® vacuum oil under this vacuum level (see Appendix Fig. A).

Alongside the SMT-fabricated samples, non-patterned coated films were fabricated under the same deposition condition without the flexography technique (i.e. no oil). These evaporated/sputtered films were then treated under the same IR or Ebeam condition, to check whether the Ebeam or IR could degrade the film performance. There was also a control group of TEGs fabricated by sputtering/evaporation through solid shadow masks as a standard to be compared with the SMT-fabricated TEG.

2.2. Sample characterisation

2.2.1. Materials characterisation

The film thickness was assessed using a *Veeco DekTak* 6 M stylus profilometer to measure a step height between uncoated and coated regions (made by polyimide tapes before deposition) on a Si wafer (L14017, *Siegert Wafer*) at six different locations.

Material phases were identified using XRD (*Rigaku Miniflex* diffractometer) with Cu k_α radiation at $2\theta = 10°–80°$, step size = 0.007°, 40 kV, 40 mA, $\lambda = 0.154$ nm.

The film crystallinity was characterised using a high vacuum *JEOL* 3000F high-resolution transmission electron microscope (TEM) under 200 keV connected to Gatan imaging filter 2000TM (1 K × 1 K and 2 K × 2 K charged coupled camera). Samples were prepared by direct deposition of films onto a lacey carbon-supported copper grid (3000 mesh, *Agar Scientific*).

Sheet resistances of films were measured using an in-house custom four-point probe system, by applying current (10^{-3}–10^{-7} A) between the outer two probes and measuring voltage in two inner probes via an *Agilent* 34420 A Nano Volt/Micro Ohm meter at 5 locations. Then, the electrical resistivity was calculated by a product of the film thickness and sheet resistance.

Mechanical tests were performed in a Linkam Scientific TST350 with a 200 N load cell, using a dog bone-like shape sample: width 10 mm × length 20 mm with a semicircle of 2 mm radius in the middle at each side.

The residual oil on an SMT specimen was imaged using a *Nikon* LV150NL optical microscope with a magnification of 5×.

The infrared absorption of the sample was recorded using a *Varian Excalibur* FTS 3500 Fourier transform infrared spectrometer with attenuated total reflection in a range of 800–5600 cm^{-1}.

Because there is fluorine (F) in *Krytox*® vacuum oil, detecting the element F in the sample could be a method to check the effect of IR and Ebeam irradiations on removing the residual oil. A *ThermoFisher Scientific* Al K_α x-ray photoelectron spectrometer (XPS) system was used.

2.2.2. Device characterisation

TEGs were characterised via an in-house built Seebeck setup using two Peltier modules (*RS* No. 693–7080) to apply a ΔT between the two sides of the TEG. The short-circuit current (I_{SC}) and open-circuit voltage (V_{OC}) were recorded by applying various ΔT in the range of 5–31 K. The Seebeck coefficient is given by the ratio of V_{OC} and ΔT. The ratio of I_{SC} and ΔT is defined herein as 'Seebeck current'. The power output was calculated ($P = U^2/R$) by measuring the voltage (U) across an external load resistor ($R_L = \sim 18$ MΩ) under a ΔT of 11.4 ± 0.2 K, which is similar to the internal resistance of the SMT-fabricated TEGs (R_{TEG}) in this case (because a maximum P can only be obtained if the load resistance equals to R_{TEG} [32–34]). (A ΔT of 11.4 K is a little smaller than the real temperature difference, 14–17 K, between the human body and room temperature, as considered a temperature loss at the contact between TEGs and the human body in a real wearable condition).

Resistances of in-line patterns (Cu and Bi—Te) were measured in a probe station using a *Keithley* 2400 meter.

The electrical contact resistance (R_c) at the interface of Cu and Bi—Te films was assessed, using the method described in [35], in a probe station with a *Keithley* 2400 source to apply current and a *Keithley* 2400 meter to measure voltage. R_c was calculated from the average voltage jump before/after the interface, using the equation:

$$R_c = A \bullet \frac{V_{jump}}{I} \quad (1)$$

where A is the contact area between semiconductor and metal (6 mm^2), V_{jump} is the voltage jump as the probes move across the interface of metal and semiconductor, I is the current applied to pass through the element (0.02 μA).

3. Results and discussion

3.1. Non-SMT fabricated samples

3.1.1. Phase identification

The purpose of using post-deposition treatment is to only remove the residual oil after SMT, without any damage to the functional coating and polymer substrate (NB: a strong post anneal, as is commonly applied to improve semiconductor performance, could improve the film performance but also could damage the polymer substrate, some such treatments on Bi—Te on polymer have been investigated in [36]). Thus, to start with, non-SMT samples (the films manufactured without oil patterns) were characterised to identify the material phase and to assess the effect of the potential oil removal treatments on the electrical performance of the films. The thicknesses of as-deposited (evaporated) Cu and (sputtered) Bi—Te films were 105 (±6) nm and 63 (±6) nm, respectively. There is no XRD peak observed for the 60-nm Bi—Te film in Fig. 2 b although the XPS result confirms the presence of Bi and Te elements and the TEM image suggests a polycrystalline structure. The Bi—Te film is too thin to obtain sufficient XRD signals. Thicker Bi—Te films (fabricated for a longer sputtering time, see Appendix Fig. B) confirmed the Bi_2Te_3 crystalline phase by XRD.

In Fig. 2 a, both XRD and XPS results confirm the phase of Cu in the evaporated film. Because the film is very thin, there is low intensity of the (1 1 1) peak. After an IR treatment under ~70 °C, there is no obvious change with increasing the annealing time (see Fig. 2 c). Short-time Ebeam treatment can slightly increase the (1 1 1) peak of Cu films, revealing that the Ebeam system is strong enough to enhance the crystallinity of as-evaporated Cu films, similarly observed in [37]. The depth of Ebeam irradiation was reported as ~50 μm [38], which could anneal the whole thickness of Cu films in this case. However, due to such a strong Ebeam, a long-time (50-min) irradiation removes the (1 1 1) peak, indicating that the film is damaged. This is also observed in an image inset Fig. 3 a, in which a 50-min Ebeam irradiation partially removes the coating of Cu, and a significant increase in resistivity is measured. These suggest that the Cu coating can be removed by a 50-min Ebeam irradiation such that the polymer substrate is exposed. The sputtered Bi—Te film seems to be less etched by the Ebeam treatment, perhaps because of the covalent nature of Bi—Te [39] and its bonding strength on PET.

3.1.2. Electrical performance

Both IR and Ebeam irradiations improved the measured electrical conductivity of as-evaporated Cu films, and the Ebeam treatment seems to be more effective (see Fig. 3 a). However, a 50-min Ebeam irradiation appears to etch the Cu film, thus increasing the electrical resistivity (thickness dependence [40]). In terms of as-sputtered Bi—Te films, there is no obvious enhancement after these post-deposition treatments. A slight apparent increase in resistivity is observed for >10-min Ebeam irradiations; such a strong Ebeam might also etch Bi—Te films, making them thinner. (The thickness used in the resistivity calculation was constant because of the limitation of the Dektak to measure e.g. <60nm Be-Te film).

This could be regarded as a further study to post-anneal a much thinner Bi—Te film (~60 nm), as contrasted to ~1-μm thick Bi—Te film [36] which was dynamically post-annealed in the Oxford webcoater by Ebeam (170 mA, 7.3 kV) or IR (~145 °C). In this study, the treatment conditions are 100 mA 4 kV (Ebeam) and ~70 °C (IR, see Appendix Fig. A) because the purpose is to only remove the residual oil without affecting the functional coating. Unlike [36], the IR radiation is not sufficient to anneal the Bi—Te film hence there is not an obvious enhancement in the film conductivity. In terms of the Ebeam treatment, again unlike [36], it does not seem to decrease (there is even a slight increase) the electrical resistivity for the ~60 nm thick Bi—Te film, because (1) the Ebeam condition in this study is not as strong as used in [36] (see above); (2) ~60 nm is close to the so-called threshold between the partially coated region and completely coated region for the room-

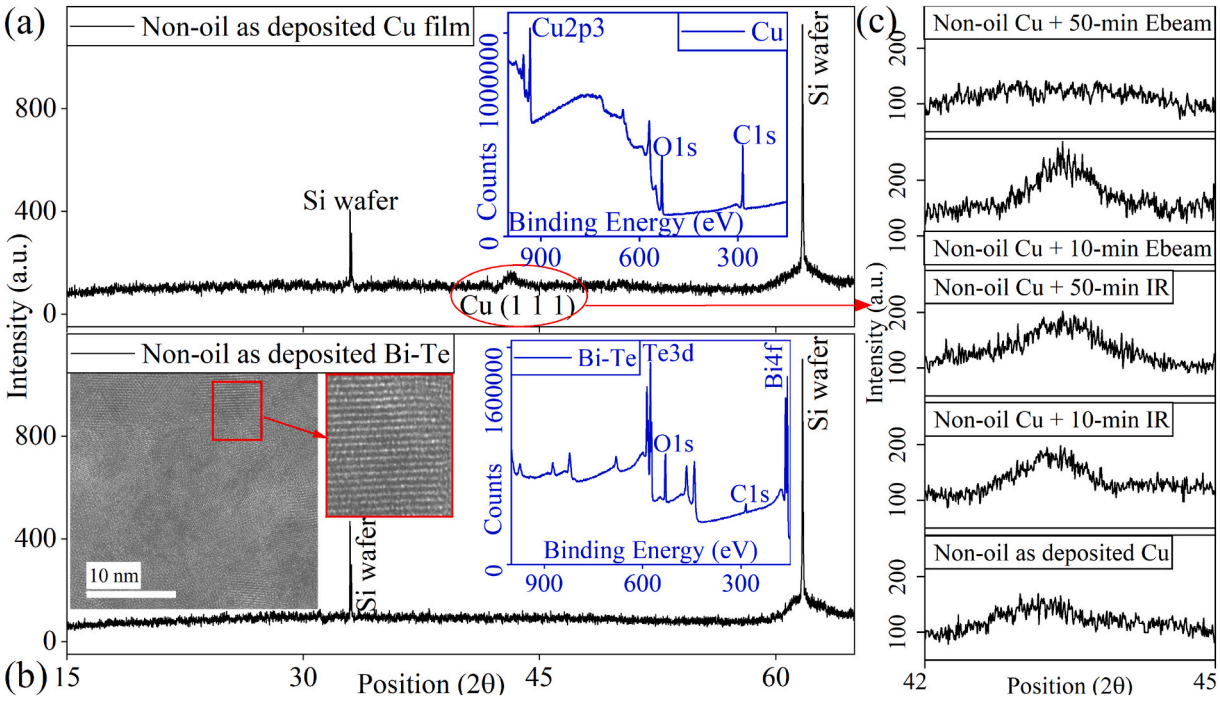

Fig. 2. (a) XRD and XPS results of the evaporated Cu film; (b) XRD, XPS and TEM results of the Bi—Te film; (c) Variations of the (1 1 1) peak in XRD of the Cu film under 10 and 50 min of Ebeam or IR treatments.

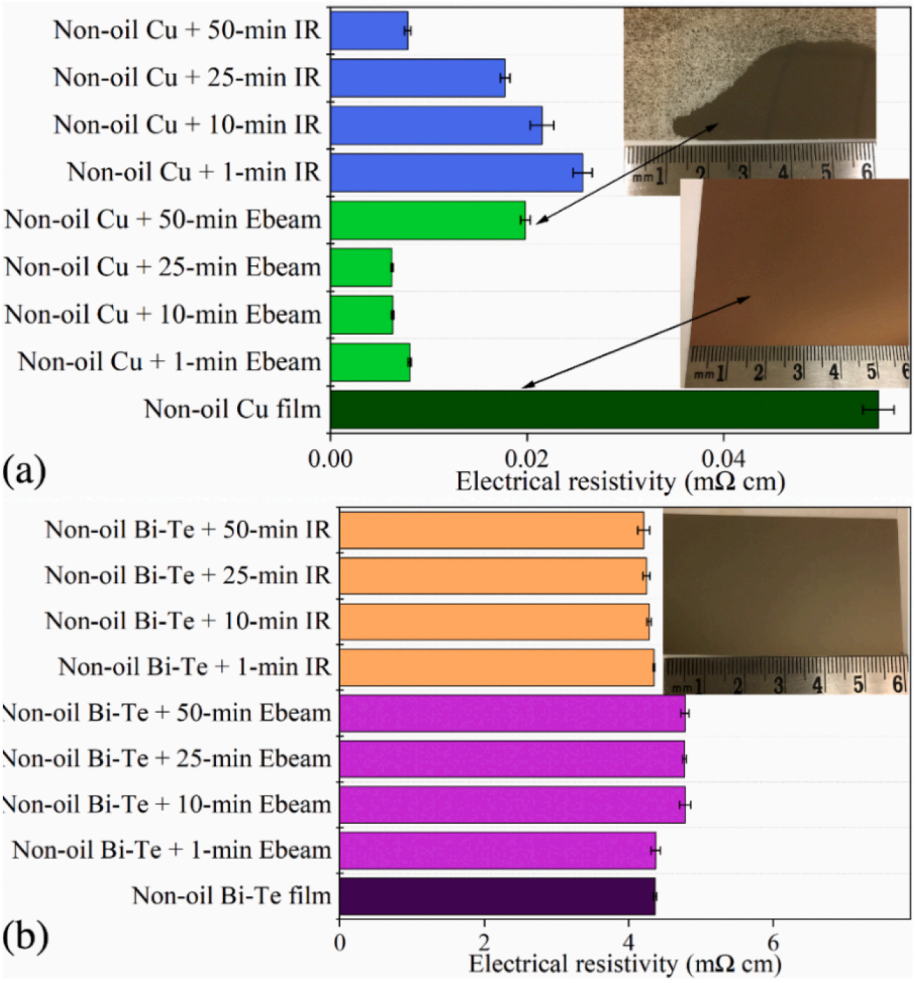

Fig. 3. Electrical resistivity of as-deposited and post-treated (a) Cu films and (b) Bi—Te films (inset: the image of the arrow pointed specimen. An etching phenomenon is only visually observed for the Cu film after a 50-min Ebeam treatment).

temperature sputtered Bi—Te film [41], hence, if the Ebeam etches the film into the partially-coated region, the electrical resistivity will increase.

The as-deposited Bi—Te film has a power factor of 3.3 (± 0.2) × 10^{-4} W m^{-1} K^{-2} with a Seebeck coefficient of −120.4 (± 3.9) μV K^{-1} (average from five identical samples) and an electrical resistivity of 4.4 (± 0.02) mΩ cm (average from five samples). A couple of Bi—Te with Cu has already been reported [29], and herein the stability is further confirmed - a negligible change in thermoelectric performance after a year (see Appendix Fig. C).

3.1.3. *Effect on mechanical performance of the substrate*

Wearable electronics should be able to undergo ~1 % strain without significant degradation of the electronic performance [42]. In terms of the flexible thin-film TEG grown on polymer sheets, the mechanical performance is dominated by the polymer substrate. A previous study examined the role of substrate properties in the resilience of these devices to the mechanical stresses that may be found during R2R production and use in wearable technologies [43]. In this study, post-deposition treatments, IR and Ebeam, are not expected to significantly influence the polymer substrate. Fig. 4 shows the result of a tensile test for untreated PET, and PET after IR/after Ebeam irradiation for ~50 min. After the irradiation by IR or Ebeam on the PET sheet, a similar Young's modulus indicates a negligible influence on the mechanical performance, as expected.

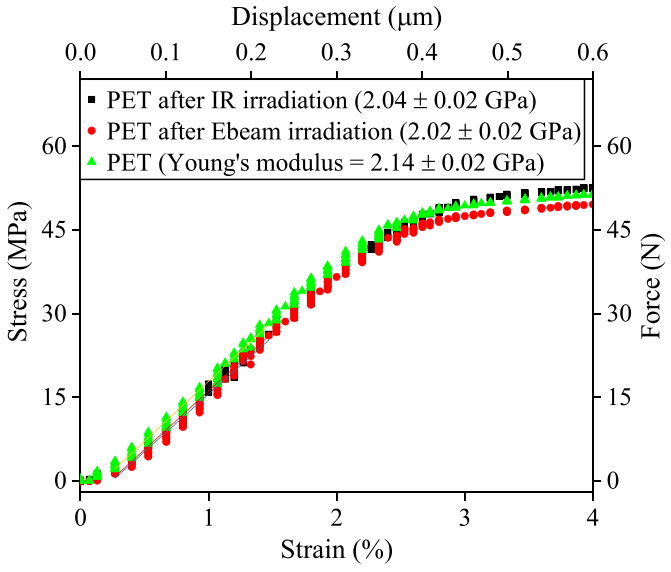

Fig. 4. Tensile stress-strain or force-displacement plot of PET with/without post-deposition treatments for ~50 min (Young's modulus is calculated by the slope below 2 % strain).

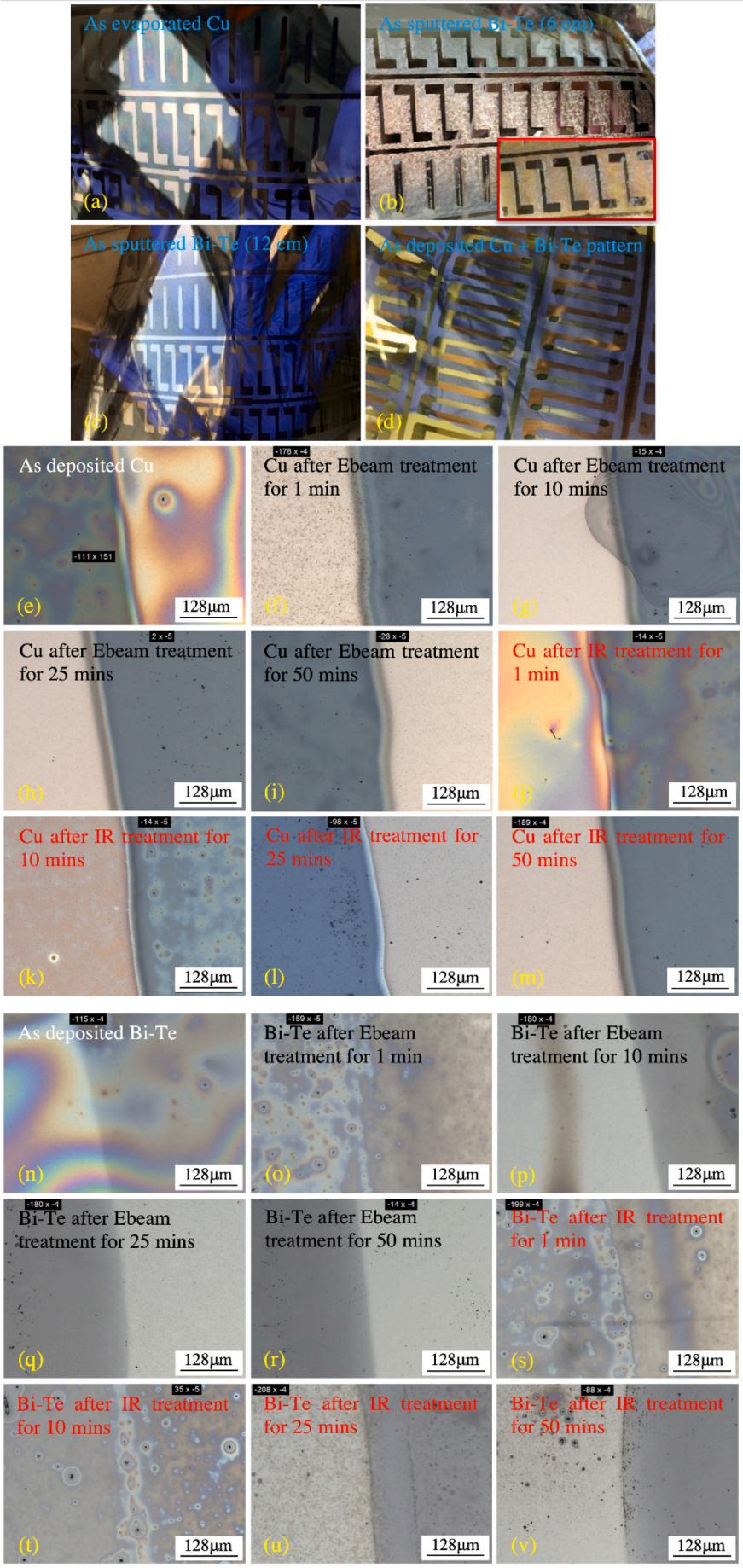

Fig. 5. Images of patterns fabricated by SMT (the strip width is 2 mm): (a) as-evaporated Cu films; (b-c) as-sputtered Bi—Te films with the source-to-substrate distances of 6-cm and 12-cm (the bright regions are directly exposed to a light source); (d) SMT-fabricated TEGs; (e-v) Cu and Bi—Te patterns after Ebeam/IR treatments for 1, 10, 25, 50 min, imaged by optical microscopy. (For e – v, the white text means the as fabricated patterns; the black means the sample after Ebeam treatment; and the red means the sample after IR treatment).

3.2. SMT-fabricated TEGs

3.2.1. Images of Cu/Bi-Te patterns

Fig. 5 a shows a clear in-line-deposited pattern of as-evaporated Cu film fabricated using SMT. A small amount of residual oil can be seen by visual observation. This is further confirmed by optical microscopy (Fig. 5 e). The residual oil was even observed in the region (see the colourful area) where the coating had been deposited. Both IR (Fig. 5 f-i) and Ebeam (Fig. 5 j-m) irradiations gradually remove the residual oil, indicating that these two treatments work well for the removal of oil from SMT-evaporated Cu samples.

Sputtered layers tend to overcoat the patterned oil creating a metal/oil surface mixture (see Fig. 5 b), as previously reported in [21]. A series of subsequent experiments were trialled to figure out this phenomenon, for example, varying the sputtering time (i.e. the film thickness), the drum rotating speed, and the sputtering power (i.e. increasing the energy of the sputtering source) to thermally remove the oil during deposition. Only increasing the target-to-substrate distance is found to work (see Fig. 5 c). The overcoating phenomenon disappears as the target-to-substrate distance is increased from 6 cm (Fig. 5 b) to 12 cm (Fig. 5 c), suggesting that (1) a shorter distance could move the substrate further into the central plasma region during sputtering, thereby all the oil pattern is under the pressure of plasma and thus there is too much local pressure for the oil to evaporate; and/or (2) the sputtered particles may have lost sufficient energy during the transfer from target to substrate, through momentum loss and interatomic collisions to allow oil to evaporate through the condensing vapour. This phenomenon is reduced (see Fig. 5 c) as the distance increases i.e. the substrate is out of the central, higher pressure, plasma region. It should be noted that a long target-to-substrate distance would decrease the sputtering rate and increase material waste. The as-deposited patterns are then post-treated for the residual oil and both IR and Ebeam are also effective to remove the residual oil in SMT-sputtered Bi—Te samples (see Fig. 5 n-v).

3.2.2. Seebeck performance of SMT-fabricated TEGs with post-deposition treatment to remove oil

Open-circuit voltage (V_{OC}) and short-circuit current (I_{SC}) are displayed with varying ΔT, showing a linear relationship where slopes of fit lines are the Seebeck coefficient and Seebeck current in Fig. 6 a and b, respectively. There is no significant change in Seebeck coefficient, while Seebeck current is significantly lower for SMT-fabricated TEGs after either IR or Ebeam irradiation, compared to a standard TEG (made by a shadow mask, i.e. non-oil fabrication). The oil seems to damage the performance of functional coatings. The internal resistances of the TEGs (R_{TEG}) measured using a probe station at room temperature are: 270 kΩ (a standard TEG fabricated by solid shadow masks without any post-deposition treatments), 25 MΩ (an SMT-Ebeam TEG), 20 MΩ (an SMT-IR TEG). These high resistances were not observed (Fig. 3) for samples exposed to the radiation treatment without oil. In terms of P output (Fig. 6 c), the SMT-fabricated TEG works even though the P is three times poorer than the standard TEG. It is noted that the external load resistance is closer to R_{TEG} of the SMT-fabricated TEG, thus the measured P is approximately the maximum of the SMT-fabricated TEG rather than the standard TEG.

R_{TEG} measured using a probe station may not be very precise because there could be an oil gap between the probe and the coating. Seebeck measurement uses a silver paste to join the leads and Cu contacts in TEGs, which may be less prone to the effects of residual oil at the

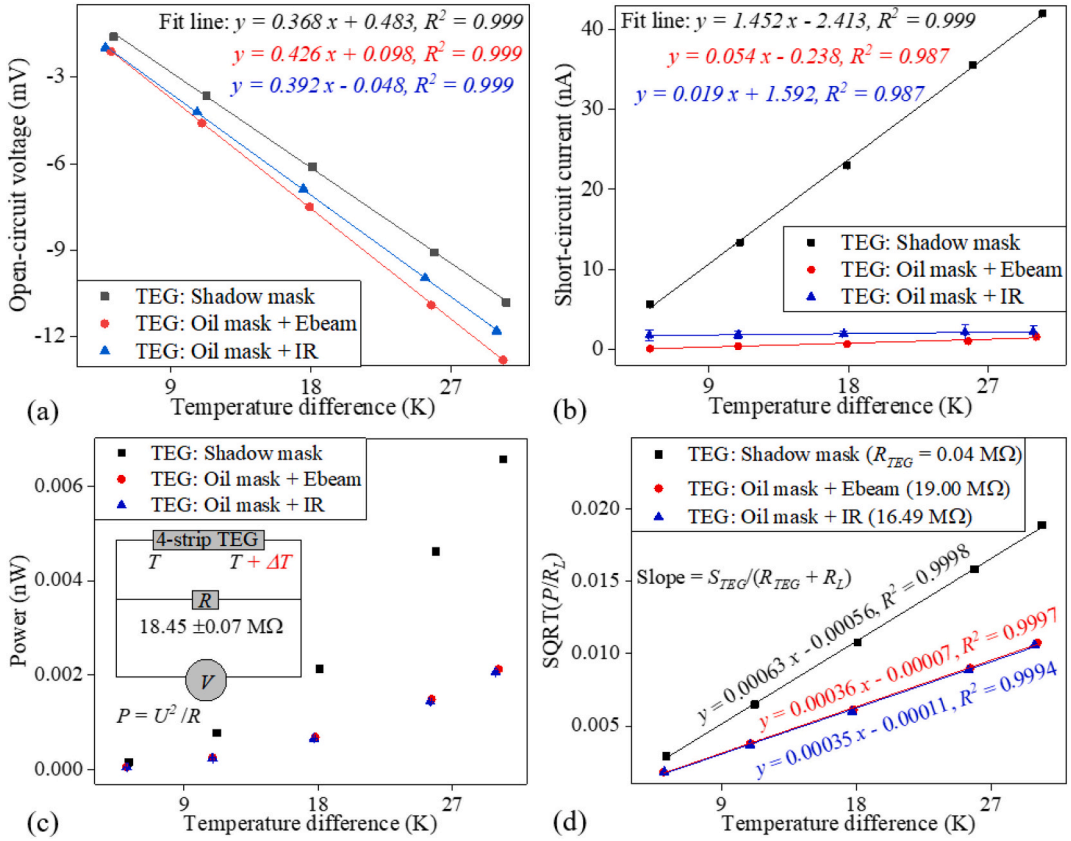

Fig. 6. (a) A plot of V_{OC} vs ΔT (slope of the linear fit is Seebeck coefficient); (b) Plot of I_{SC} vs ΔT (slope of the linear fit is defined as Seebeck current herein); (c) P output of TEGs (the dimension of TE strip is 13 mm × 2 mm); (d) Plot to calculate R_{TEG} through the linear fit. (Specimens contain four Bi—Te strips. The Ebeam and IR irradiations are 25 min.)

contact. To further confirm R_{TEG}, the data of P is used to calculate R_{TEG} under a ΔT, using the following equation [34]:

$$P = I^2 \bullet R_L = \left(\frac{S_{TEG} \bullet \Delta T}{R_{TEG} + R_L}\right)^2 \bullet R_L \quad (2)$$

rearranged to:

$$\sqrt{\frac{P}{R_L}} = \frac{S_{TEG}}{R_{TEG} + R_L} \Delta T \quad (3)$$

where R_L is the load resistance (18.45 MΩ), S_{TEG} is Seebeck coefficient of the whole device (i.e. the slope in Fig. 6 a), ΔT is the temperature difference (11.4 K), R_{TEG} is the internal resistance of the whole device.

The calculated R_{TEG} under ΔT (see Fig. 6 d) again indicates that oil significantly affects the performance of functional films, and thus a significant difference is observed in Fig. 6b. Fig. 6a reveals that the R2R SMT-manufactured TEG has a comparable voltage output to the standard TEG, and thus can be used for portable devices requiring a voltage-dominant source. To behave as a power source, the SMT-fabricated TEG (Fig. 6 c) is more suitable for portable devices with an extremely large resistance (in the MΩ range).

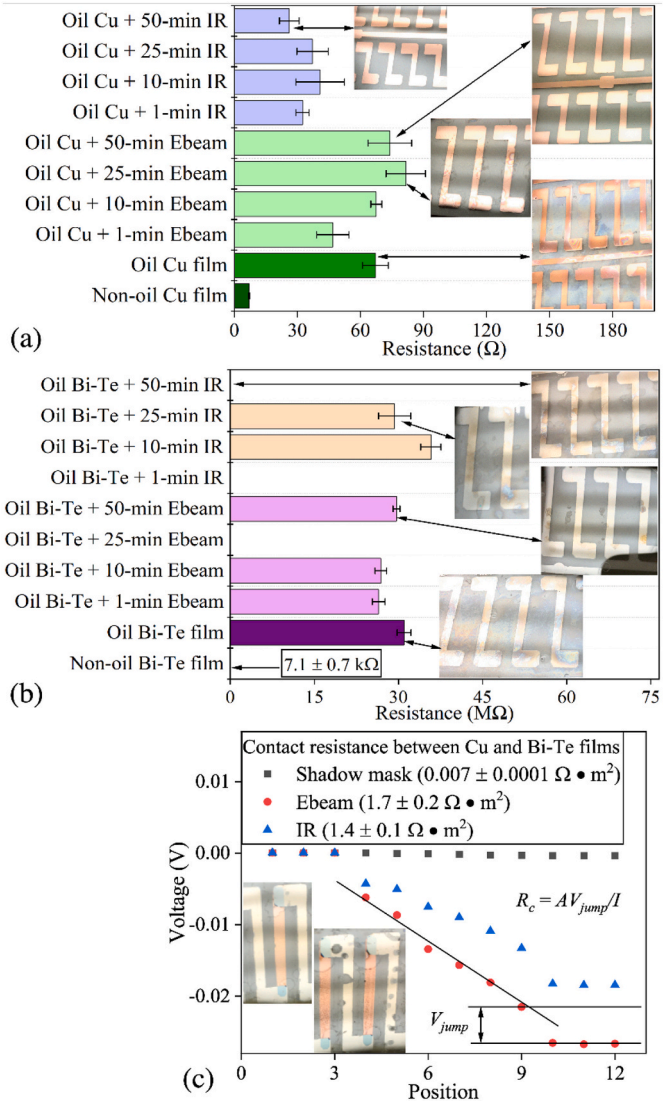

Fig. 7. (a & b) Resistances of SMT-fabricated Cu and Bi—Te strips (13 mm × 2 mm), following IR or Ebeam irradiations with different annealing times; (c) R_C of Cu/Bi-Te interface of a standard TEG and SMT-fabricated TEGs following 25-min IR and Ebeam treatments (the standard deviation is from three measurements).

3.2.3. *Why does R_{TEG} increase using SMT?*

IR and Ebeam treatments are not expected to significantly affect R_{TEG}, as analysed from Fig. 3 for non-SMT-fabricated samples. However, R_{TEG} changes a lot for SMT-fabricated and cleaned samples. Resistances of SMT-fabricated strips (2 mm × 13 mm) were measured using a probe station, as shown in Fig. 7a and b. The oiled Cu film (67 Ω) has a much higher (~10 times) resistance than non-oiled Cu film (7 Ω). Post-deposition treatments (IR and Ebeam) should gradually decrease the resistance of oiled Cu film with the annealing time. However, the trend is not obvious, and some samples with a long-time anneal even have a higher resistance than the original oiled Cu film. Diffusion of oil into the film region is observed in Fig. 5. Given the scatter in the results in Fig. 7a, it is speculated that the oil thickness is not even. This is particular to the case in which a single drum rotates. It is predicted that, in a real R2R case, the residual oil will uniformly cover the film region after the polymer web passes a series of rollers, rapidly moving away from the oiling region. Hence, it is predicted that the thickness of residual oil could likely be removed at a linear speed with the annealing time, thus reducing resistance. In addition, during an R2R process, if the residual oil is so thin that the cleaning technique can rapidly remove it, then the residual oil will not diffuse to the coated region. However, the resistance of the Cu film is not significant in TEGs because R_{TEG} is dominated by the TE (semiconductor) part, so this observed change in the Cu resistance is likely not significant to the device performance.

In Fig. 7b, it is seen that resistance of the Bi—Te strip dramatically increases for SMT/oiled Bi—Te films (in the MΩ range), compared to non-oiled films (the standard sample in the kΩ range). Some Bi—Te strips are even unmeasurable.

Doping and oxidation are considered possible causes of the high resistance in SMT-fabricated films. *Krytox*® oil contains carbon, oxygen and fluorine. XPS was used to check the residual F (Fluorine) on the film after post-anneals (see Fig. 8 and Table 1). F is found in both Cu and Bi—Te films even after 50-min post-deposition treatments. Ebeam irradiation gradually decreases the amount of observed F (see atomic% in Table 1) with the treatment time for both Cu and Bi—Te films. Removal of the F using IR seems to work for the Cu film but not well for the Bi—Te film. This could be because IR annealing could cause a reaction between F and Bi—Te films and thus F will never be removed by the IR irradiation. The existence of F in the Cu film does not change their electrical performance too much, because TEGs only require the Cu contacts to be conductive in the Ω range. However, there is a severe phenomenon for the Bi—Te semiconductor because doping of F in a Bi—Te film seems to significantly degrade the electrical performance, R_{TEG} (see Fig. 6 b and d). Oxidation is another consideration in terms of an increase in R_{TEG}. Both Bi and Te elements could be oxidised: a big oxidation peak is observed in Fig. 8 e and f. The influence of oxygen content on the TE performance of the Bi-Te-based film has already been reported [44].

In addition to a possible doping or oxidation issue in Bi—Te films, the junction between Cu and Bi—Te films is also analysed. Images inset Fig. 7 c indicate the region of the oil pattern is not uniform. After SMT-evaporated Cu patterns are post-annealed, the residual oil may not be completely removed, prior to deposition of the Bi—Te patterns. A breakage in the Bi—Te pattern of the strip was observed (see Fig. 7 c inset image) because the Bi—Te film cannot grow onto the residual oil region. Only true patterns of SMT-fabricated TEGs are selected for analysis through this study. In terms of the Cu/Bi-Te junction, oil could also exist at the interface. The contact resistance, R_c, of SMT-fabricated TEG is about 200-times larger than that of the standard TEG (Fig. 7 c). Hence, a layer of oil or F possibly exists between Cu and Bi—Te coatings.

Overall, the residual oil could dope or oxidise the functional coating, especially in Bi—Te films. A sandwich structure, Cu/Oil/Bi-Te, could exist at the interface. These two phenomena result in an increase in R_{TEG} of the SMT- fabricated TEG.

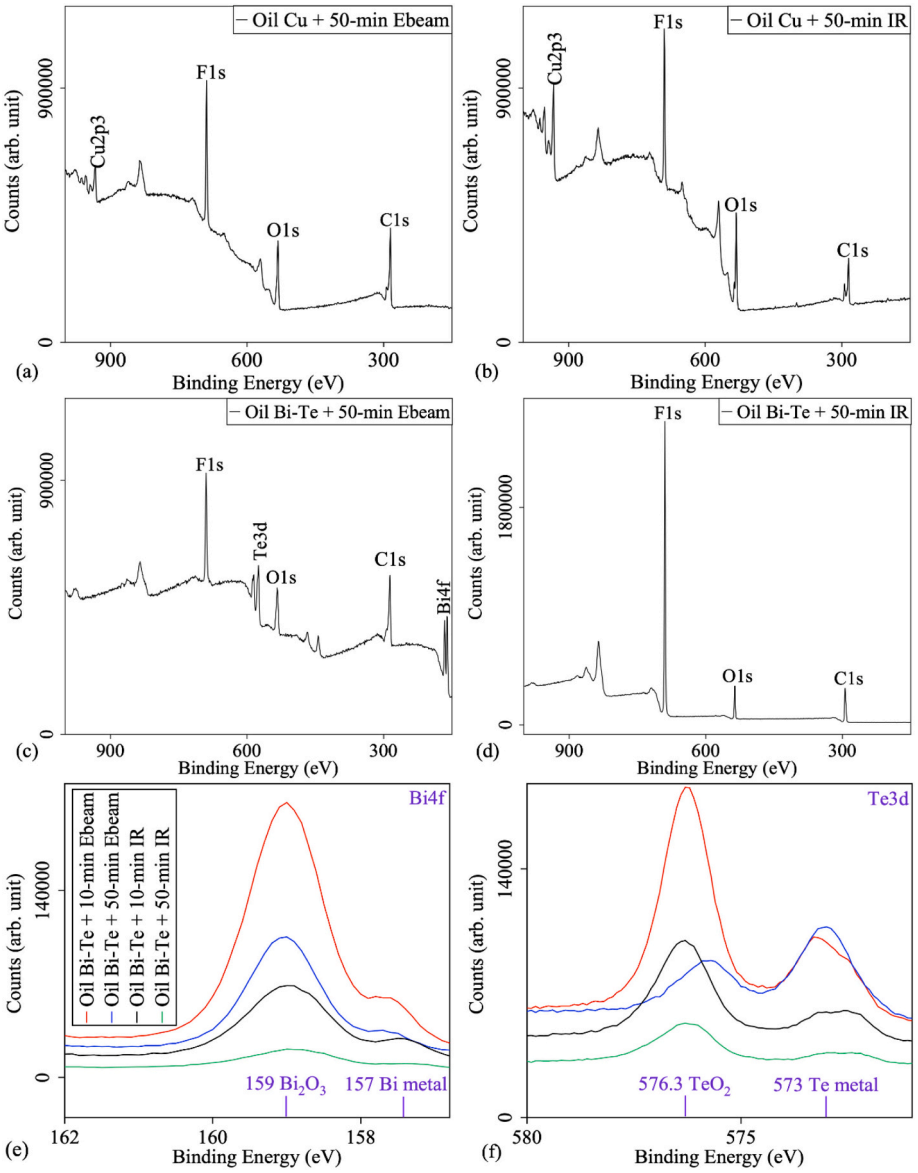

Fig. 8. XPS results of SMT-fabricated patterns after IR or Ebeam treatment.

Table 1
Elemental compositions of SMT-fabricated samples after IR/Ebeam treatments as determined from XPS.

Atomic%	F	Cu	Bi	Te	O	C
Oil Cu + 10-min Ebeam	44.33	4.24	–	–	18.19	33.27
Oil Cu + 50-min Ebeam	26.55	3.47	–	–	52.38	17.6
Oil Cu + 10-min IR	61.42	0.35	–	–	9.6	28.63
Oil Cu + 50-min IR	28.97	7.38	–	–	26.39	37.27
Oil Bi-Te + 10-min Ebeam	54.52	–	2.2	2.17	14.67	26.45
Oil Bi-Te + 50-min Ebeam	23.85	–	1.51	1.78	15.25	57.61
Oil Bi-Te + 10-min IR	62.16	–	0.07	0.19	9.34	28.24
Oil Bi-Te + 50-min IR	62.52	–	0.03	0.08	9.4	28.01

4. Conclusion

Selective metallisation by sputtering and evaporation was explored to fabricate flexible thin-film TEGs in a roll-to-roll process. To deposit a two-layer device by oil printing, two post-deposition cleaning methods (electron beam and infrared) were studied to remove the residual oil of the first layer before deposition of the second layer. The fabricated TEG works and behaves as a voltage-dominant source, comparable to a standard TEG fabricated using a shadow mask, but the power performance is much poorer than the standard device because the internal resistance increases dramatically. This could be ascribed to the effect of the oil by (1) oxidation/doping of fluorine in the functional coatings; (2) residual oil at the metal-semiconductor interface. Further investigations of the oil type, precise control of oil pattern and stronger Ebeam or IR

irradiations are considered in the future.

CRediT authorship contribution statement

Xudong Tao: Conceptualization, Investigation, Writing – original draft. **Bryan W. Stuart:** Methodology, Writing – review & editing. **Hazel E. Assender:** Supervision, Writing – review & editing.

Declaration of competing interest

The authors declare that they have no known competing financial interests or personal relationships that could have appeared to influence the work reported in this paper.

Data availability

Data will be made available on request.

Acknowledgement

The authors would like to acknowledge the foundation from Engineering and Physical Sciences Research Council [grant number EP/M015173/1]. Especially thanks to Dr. Philip Holdway, Ms. Yu Shu and Mr. Botao Hao for their help with XPS, optical microscopy and TEM, respectively. The authors are also grateful to the equipment access from Oxford Materials Characterisation Services and Oxford Materials and David Cockayne Centre and to DuPont Teijin films for the supply of polymer substrates.

Appendix A

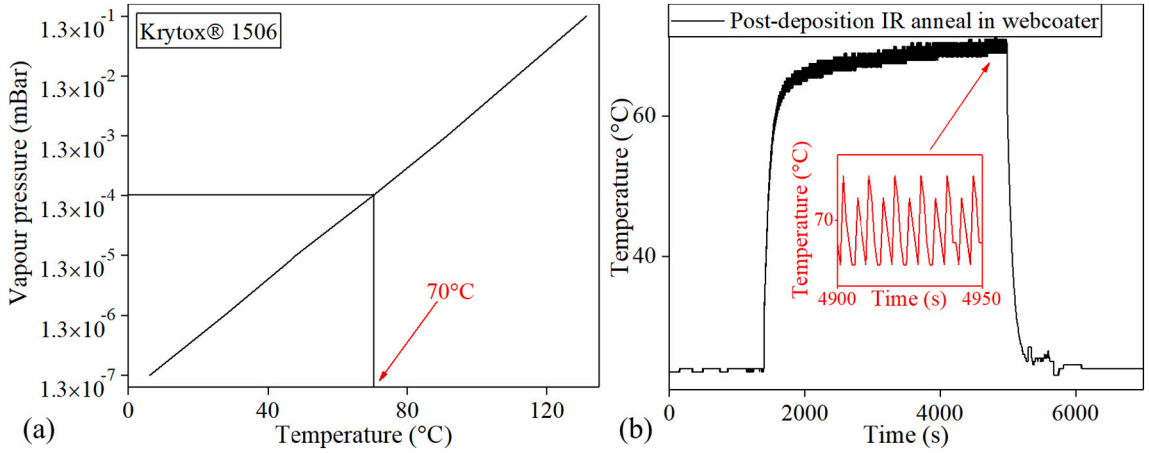

Fig. A. (a) Plot of vapour pressure and temperature of Krytox® 1506 vacuum oil; (b) Temperature recording of IR source in web coater (a thermocouple was attached on the drum which rotated at a speed of 25 m min^{-1} at the drum surface, hence the thermocouple passed the IR source every 4.32 s. The temperature number fluctuates around 70 °C as the drum rotates).

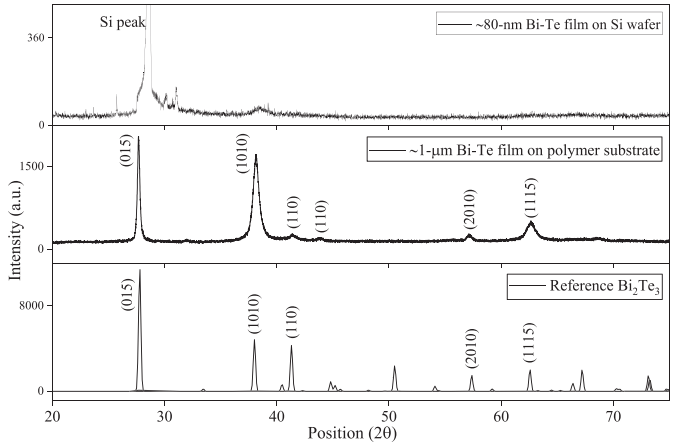

Fig. B. XRD pattern of ~80-nm film grown on a Si wafer and ~1-μm Bi—Te film grown on a polymer substrate, with the references of Bi_2Te_3 (ICSD #193330) powders.

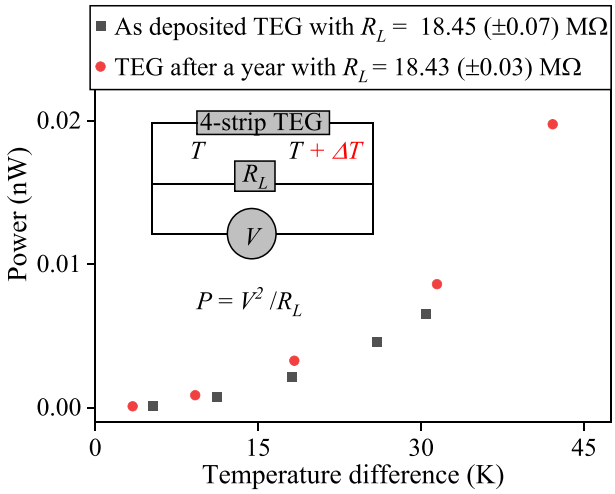

Fig. C. Power results of TEG (shadow mask): as deposited and after a year.

References

[1] S. Lee, Q. Shi, C. Lee, From flexible electronics technology in the era of IoT and artificial intelligence toward future implanted body sensor networks, APL Mater. 7 (2019) 031302–031313, https://doi.org/10.1063/1.5063498.

[2] N. Palavesam, S. Marin, D. Hemmetzberger, C. Landesberger, K. Bock, C. Kutter, Roll-to-roll processing of film substrates for hybrid integrated flexible electronics, in: Flexible and Printed Electronics 3, 2018, https://doi.org/10.1088/2058-8585/aaaa04.

[3] G.C. Glatzmaier, J. Rea, M.L. Olsen, C. Oshman, C. Hardin, J. Alleman, J. Sharp, R. Weigand, D. Campo, G. Hoeschele, P.A. Parilla, N.P. Siegel, E.S. Toberer, D. S. Ginley, Solar thermoelectricity via advanced latent heat storage: a cost-effective small-scale CSP application, AIP Conf Proc. 1850 (2017), 300191, https://doi.org/10.1063/1.4984362.

[4] H. Noro, K. Sato, H. Kagechika, The thermoelectric properties and crystallography of Bi-Sb-Te-Se thin films grown by ion beam sputtering, J. Appl. Phys. 73 (1993) 1252–1260, https://doi.org/10.1063/1.353266.

[5] D. Kim, E. Byon, G. Lee, S. Cho, Effect of deposition temperature on the structural and thermoelectric properties of bismuth telluride thin films grown by co-sputtering, Thin Solid Films 510 (2006) 148–153, https://doi.org/10.1016/j.tsf.2005.12.306.

[6] H. Huang, W. Luan, S. Tu, Influence of annealing on thermoelectric properties of bismuth telluride films grown via radio frequency magnetron sputtering, Thin Solid Films 517 (2009) 3731–3734, https://doi.org/10.1016/j.tsf.2009.01.015.

[7] Y. Zhou, L. Li, Q. Tan, J. Li, Thermoelectric properties of Pb-doped bismuth telluride thin films deposited by magnetron sputtering, J. Alloys Compd. 590 (2014) 362–367, https://doi.org/10.1016/j.jallcom.2013.12.136.

[8] W. Qu, M. Plötner, W. Fischer, Microfabrication of thermoelectric generators on flexible foil substrates as a power source for autonomous microsystems, J. Micromech. Microeng. 11 (2001) 146, https://doi.org/10.1088/0960-1317/11/2/310.

[9] Y. Du, J. Xu, B. Paul, P. Eklund, Flexible thermoelectric materials and devices, Appl. Mater. Today 12 (2018) 366–388, https://doi.org/10.1016/j.apmt.2018.07.004.

[10] Pilaipon Nuthongkum, Rachsak Sakdanuphab, Mati Horprathum, Aparporn Sakulkalavek, [Bi]:[Te] control, structural and thermoelectric properties of flexible Bi^sub x^Te^sub y^ thin films prepared by RF magnetron sputtering at different sputtering pressures, J. Electron. Mater. 46 (2017) 6444–6450, https://doi.org/10.1007/s11664-017-5671-x.

[11] L.M. Goncalves, C. Couto, P. Alpuim, A.G. Rolo, F. Völklein, J.H. Correia, Optimization of thermoelectric properties on Bi2Te3 thin films deposited by thermal co-evaporation, Thin Solid Films 518 (2010) 2816–2821, https://doi.org/10.1016/j.tsf.2009.08.038.

[12] C.A. Bishop, E.M. Mount, in: 15 - Vacuum Metallizing for Flexible Packaging, Multilayer Flexible Packaging, 2016, pp. 235–255, https://doi.org/10.1016/B978-0-323-37100-1.00015-6.

[13] Z. Cao, E. Koukharenko, M.J. Tudor, R.N. Torah, S.P. Beeby, Screen Printed Flexible Bi2Te3-Sb2Te3 Based Thermoelectric Generator, 1970, https://doi.org/10.1088/1742-6596/476/1/012031.

[14] S. Shin, R. Kumar, J.W. Roh, D. Ko, H. Kim, S.I. Kim, L. Yin, S.M. Schlossberg, S. Cui, J. You, S. Kwon, J. Zheng, J. Wang, R. Chen, High-performance screen-printed thermoelectric films on fabrics, Sci. Rep. 7 (2017) 7317–7319, https://doi.org/10.1038/s41598-017-07654-2.

[15] B. Chen, M. Kruse, B. Xu, R. Tutika, W. Zheng, M.D. Bartlett, Y. Wu, J.C. Claussen, Flexible thermoelectric generators with inkjet-printed bismuth telluride nanowires and liquid metal contacts, Nanoscale 11 (2019) 5222–5230, https://doi.org/10.1039/c8nr09101c.

[16] D. Madan, Z. Wang, P.K. Wright, J.W. Evans, Printed flexible thermoelectric generators for use on low levels of waste heat, Appl. Energy 156 (2015) 587–592, https://doi.org/10.1016/j.apenergy.2015.07.066.

[17] T. Cosnahan, A.A.R. Watt, H.E. Assender, Modelling of a vacuum metallization patterning method for organic electronics, Surface & Coatings Technology. 336 (2018) 128–132, https://doi.org/10.1016/j.surfcoat.2017.09.058.

[18] M.J. Madou, in: Manufacturing Techniques for Microfabrication and Nanotechnology, CRC Press, 2011, pp. 403–404, https://doi.org/10.1201/9781439895306.

[19] Taylor, Cliffordl, Bjornard, Erikj, Valiska, Michaelj, in: Film Thickness Uniformity Control Apparatus for In-line Sputtering Systems, US Patents, 1992, pp. 1–7. https://patents.google.com/patent/US515672.

[20] Z. Wei, P.R. Bobbili, S. Senthilarasu, T. Shimell, H.M. Upadhyaya, Design and optimisation of process parameters in an in-line CIGS evaporation pilot system, Surf. Coat. Technol. 241 (2014) 159–167, https://doi.org/10.1016/j.surfcoat.2013.10.033.

[21] B.W. Stuart, X. Tao, D. Gregory, H.E. Assender, roll-to-roll patterning of Al/Cu/Ag electrodes on flexible polyethylene by oil masking: a comparison of thermal evaporation and magnetron sputtering, Appl. Surf. Sci. 505 (2019), 144294, https://doi.org/10.1016/j.apsusc.2019.144294.

[22] J. Kim, J. Choi, J. Bae, M. Kim, T. Oh, Thermoelectric characteristics of n-type Bi2Te3 and p-type Sb2Te3 thin films prepared by co-evaporation and annealing for thermopile sensor applications, Mater. Trans. 54 (2013) 618–625, https://doi.org/10.2320/matertrans.M2013010.

[23] C. Sudarshan, S. Jayakumar, K. Vaideki, C. Sudakar, Effect of vacuum annealing on structural, electrical and thermal properties of e-beam evaporated Bi2Te3 thin films, Thin Solid Films 629 (2017) 28–38, https://doi.org/10.1016/j.tsf.2017.03.043.

[24] K. Singkaselit, A. Sakulkalavek, R. Sakdanuphab, Effects of annealing temperature on the structural, mechanical and electrical properties of flexible bismuth telluride thin films prepared by high-pressure RF magnetron sputtering, Ansn. 8 (2017) 350021–350027, https://doi.org/10.1088/2043-6254/aa7222.

[25] T. Nishino, T. Suzuki, Flexible thermoelectric generator with efficient vertical to lateral heat path films, J. Micromech. Microeng. 27 (2017) 35011, https://doi.org/10.1088/1361-6439/aa5aad.

[26] D. Takemori, M. Okuhata, M. Takashiri, Thermoelectric properties of electrodeposited bismuth telluride thin films by thermal annealing and homogeneous electron beam irradiation, ECS Trans. 75 (2017) 123–131, https://doi.org/10.1149/07552.0123ecst.

[27] Y. Ding, Y. Qiu, K. Cai, Q. Yao, S. Chen, L. Chen, J. He, High performance n-type Ag2Se film on nylon membrane for flexible thermoelectric power generator, Nat. Commun. 10 (2019) 1–7, https://doi.org/10.1038/s41467-019-08835-5.

[28] V. Karthikeyan, J.U. Surjadi, J.C.K. Wong, V. Kannan, K. Lam, X. Chen, Y. Lu, V.A. L. Roy, Wearable and flexible thin film thermoelectric module for multi-scale energy harvesting, J. Power Sources 455 (2020), 227983, https://doi.org/10.1016/j.jpowsour.2020.227983.

[29] X. Tao, K. Zhang, D. Gregory, J. Liu, H.E. Assender, Device optimization and large-scale roll-to-roll manufacturability of flexible thin-film thermoelectric generators, Energy Technol. (Weinheim, Germany) 9 (2021) n/a, https://doi.org/10.1002/ente.202001008.

[30] L. Francioso, C. De Pascali, I. Farella, C. Martucci, P. Cretì, P. Siciliano, A. Perrone, Flexible thermoelectric generator for ambient assisted living wearable biometric sensors, J. Power Sources 196 (2011) 3239–3243, https://doi.org/10.1016/j.jpowsour.2010.11.081.

[31] X. Tao, K. Wan, B.W. Stuart, E. Bilotti, H.E. Assender, BixTey thermoelectric thin films sputtered at room temperature onto moving polymer web: effect of gas pressure on materials properties, Thin Solid Films 712 (2020), 138311, https://doi.org/10.1016/j.tsf.2020.138311.
[32] F. Suarez, A. Nozariasbmarz, D. Vashaee, M.C. Öztürk, in: Designing Thermoelectric Generators for Self-powered Wearable Electronics 9, 2016, pp. 299–2113, https://doi.org/10.1039/c6ee00456c.
[33] M. Hodes, Optimal pellet geometries for thermoelectric power generation, IEEE Trans. Components Packag. Technol. 33 (2010) 307–318, https://doi.org/10.1109/TCAPT.2009.2039934.
[34] D. Enescu, Thermoelectric energy harvesting: basic principles and applications, Green Energy Adv. (2019), https://doi.org/10.5772/intechopen.83495.
[35] W. Liu, H. Wang, L. Wang, X. Wang, G. Joshi, G. Chen, Z. Ren, Understanding of the contact of nanostructured thermoelectric n-type Bi2Te2.7Se0.3 legs for power generation applications, J. Mater. Chem. A 1 (2013) 13093, https://doi.org/10.1039/c3ta13456c.
[36] X. Tao, B.W. Stuart, K. Wan, J.W. Murray, E. Bilotti, H.E. Assender, Static and dynamic postannealing strategies for roll-to-roll fabrication of DC magnetron sputtered bismuth telluride thin films onto polymer webs, ACS Appl. Mater. Interfaces 13 (2021) 10149–10160, https://doi.org/10.1021/acsami.1c00721.
[37] S. Kudo, S. Tanaka, K. Miyazaki, Y. Nishi, M. Takashiri, Anisotropic analysis of nanocrystalline bismuth telluride thin films treated by homogeneous electron beam irradiation, Mater. Trans. 58 (2017) 513–519, https://doi.org/10.2320/matertrans.M2016295.
[38] M. Takashiri, M. Uyama, K. Imai, Comparison of crystal growth and thermoelectric properties of n-type bi-se-Te and p-type bi-sb-Te nanocrystalline thin films: effects of homogeneous irradiation with an electron beam, J. Appl. Phys. 115 (2014) 2143111–2143117, https://doi.org/10.1063/1.4881676.
[39] T. Ludwig, L. Guo, P. McCrary, Z. Zhang, H. Gordon, H. Quan, M. Stanton, R. M. Frazier, R.D. Rogers, H. Wang, C.H. Turner, Mechanism of bismuth telluride exfoliation in an ionic liquid solvent, Langmuir 31 (2015) 3644–3652, https://doi.org/10.1021/acs.langmuir.5b00239.
[40] E. Schmiedl, P. Wissmann, H. Finzel, The electrical resistivity of ultra-thin copper films, Zeitschrift Für Naturforschung. A, J. Phys. Sci. 63 (2008) 739–744, https://doi.org/10.1515/zna-2008-10-1118.
[41] X. Tao, K. Wan, J. Deru, E. Bilotti, H.E. Assender, Thermoelectric behaviour of bi-Te films on polymer substrates DC-sputtered at room-temperature in moving web deposition, Surf. Coat. Technol. 385 (2020), 125393, https://doi.org/10.1016/j.surfcoat.2020.125393.
[42] D. Kim, J.A. Rogers, Stretchable electronics: materials strategies and devices, Adv. Mater. 20 (2008) 4887–4892, https://doi.org/10.1002/adma.200801788.
[43] X. Tao, K. Zhang, B.W. Stuart, H.E. Assender, Elastic (acrylate/polydimethylsiloxane) substrate-to-coating interlayers for improving the mechanical resilience of thermoelectric films on poly(ethylene terephthalate) during roll-to-roll manufacture and in service operation, Surf. Coat. Technol. 434 (2022), 128167, https://doi.org/10.1016/j.surfcoat.2022.128167.
[44] Y. Horio, A. Inoue, Effect of oxygen content on thermoelectric properties of n-type (Bi, Sb)2(Te, Se)3 alloys prepared by rapid solidification and hot-pressing techniques, Mater. Trans. 47 (2006) 1412–1416, https://doi.org/10.2320/matertrans.47.1412.